Allogenic and autogenic effects on mangrove dynamics from the Ceará Mirim River, Northeastern Brazil, during the middle and late Holocene

Samuel Rodrigues Ribeiro[a], Edson José Louzada Batista[a], Marcelo C. L. Cohen[a*],

Marlon Carlos França[b] Luiz C.R. Pessenda[c], Neuza A. Fontes[a], Igor C. C. Alves[a],

José A. Bendassolli[d],

[a] Federal University of Pará, Graduate Program of Geology and Geochemistry, Laboratory of Coastal Dynamics. Rua Augusto Corrêa, 01 - Guamá. CEP 66075-110, Belém (PA), Brazil.

[b] Federal Institute of Pará, Av. Alm. Barroso, 1155, Marco, 66090-020, Belém (PA), Brazil.

[c] University of São Paulo, CENA/[14]C Laboratory, Av. Centenário 303, 13400-000, Piracicaba, São Paulo, Brazil.

[d] University of São Paulo, CENA/Stable Isotopes Laboratory, Av. Centenário 303, 13400-000, Piracicaba, São Paulo

*Corresponding author: Marcelo Cancela Lisboa Cohen

Federal University of Pará - Brazil

Rua Augusto Corrêa, 01 - Guamá. CEP 66075-110, Belém (PA), Brazil.

Tel.: +55 91 3201-7988

E-mail address: mcohen80@hotmail.com

Abstract

It is possible that climate changes and sea level fluctuations (allogenic processes) are and will cause major changes in the mangrove dynamics. However, other driving forces may be significantly affecting this system. Distinguishing allogenic and autogenic influence on mangroves is a challenging question, because mechanisms related to the natural dynamics of depositional environments (autogenic processes) have strong influences on the establishment and degradation of mangroves. Thus, impacts on mangroves caused by autogenic processes may be erroneously attributed to allogenic mechanisms. Therefore, it is imperative to identify the "fingerprint" of global changes in modern mangrove dynamics. In order to characterize the influence of these forces on mangroves, this work has used geomorphology and vegetation maps integrated with sedimentological and palynological data, radiocarbon dating, as well as δ^{13}C, δ^{15}N and C/N from sedimentary organic matter. The inter-proxy analyses reveal an estuarine influence with mangrove development along the Ceará Mirim River, Northeastern Brazil, since ~6920 cal yr BP, after the post-glacial sea level rise. Relative Sea Level (RSL) has been stable during the middle and late Holocene. Mangrove establishment along this fluvial valley begins at about 6920 cal yr BP, caused by the sea-level stabilization, an allogenic influence. However, after its establishment, wetland dynamics were mainly controlled by autogenic factors, related to channel migrations, instead of allogenic process. Some influence of sea-level and climate changes on mangrove dynamics in this estuarine channel have been weakened by more intense tidal channels activities. Therefore, the expansion and contraction of mangrove areas along the estuary of the Ceará Mirim River since 6920 cal yr BP has been mainly influenced by channel dynamics that regulate the accretion and erosion of mangrove substrates.

Introduction

Multi-proxy analyses reveal that marine influence and mangrove vegetation areas were more extensive than today on the mouth of Amazon River during the middle Holocene, forming a continuous mangrove belt along the northern Brazilian Amazon littoral. The establishment of this mangrove strip is a direct consequence of the marine incursion caused by post-glacial sea-level rise. In the late Holocene (<4.2 ka BP), in areas influenced by the Amazon River discharge, the mangroves were replaced by freshwater vegetation. Likely, the fragmentation of this continuous mangrove line was caused by the increase of fluvial discharge associated to the change from dry into wet climates, which caused a significant decrease of tidal water salinity in areas near the mouth of Amazon River, during the late Holocene. (Cohen et al., 2012).

According to Boski et al. (2015), the post-transgression period in the Rio Grande do Norte, northeastern Brazilian littoral (Fig. 1a), witnessed the decline of mangroves. Accelerated sea-level rise combined with geomorphological confinement of the studied intertidal zone was probably responsible for the demise of halophyte vegetation, which thrived again in the late Holocene. However, its vanishing could be resulted from the combined stress of sea-level rise and a dryer climatic phase.

Regarding the southeastern Brazilian coast (Fig. 1a), the geomorphology is mainly related to sea-level changes (Rossetti et al., 2015). Sea-level fall of the Last Glacial Maximum produced a coastal progradation with beach ridges and deltaic deposits. Post-glacial sea-level rise generated embayments, estuaries and lagoons.

This event crossed the paleoshoreline, ultimately reactivating estuaries previously abandoned over the Barreiras Formation in the continental area. Stratigraphic sequences from these estuaries indicated brackish conditions and expansion of mangroves up to the mid-Holocene. These water bodies gradually became completely continental-influenced, consequently the mangroves almost disappeared as they migrated seaward during the late Holocene (Castro et al., 2013; Marcelo Cancela Lisboa Cohen et al., 2014; França et al., 2015, 2012; Lorente et al., 2014; Rossetti et al., 2015).

Therefore, along the northern Brazil (Fig. 1c), the mangrove dynamics has been controlled mainly by the climate and RSL changes (Behling et al., 2004; Cohen et al., 2012; França et al., 2012; Guimarães et al., 2012; Lara and Cohen, 2009; Smith et al., 2012), while in southeastern Brazil (Fig. 1c), Espírito Santo, Rio de Janeiro and São Paulo's States, the displacement of mangroves would be mainly related to RSL changes (M.C.L. Cohen et al., 2014; Lorente et al., 2013; Pessenda et al., 2012).

In this context, after the post-glacial sea-level rise, the RSL reached the current level between 7800 and 6600 cal yrs BP, and a highstand (2 - 5 m) at about 5500 cal BP between Santa Catarina and Rio Grande do Norte (Angulo et al., 2006 - fig. 1a, sector G; Castro *et al.*, 2014; Martin et al. (2003) - fig. 1a, sector F; Suguio et al. (2013), fig. 1a, sector D). The RSL decreased continually during the late Holocene (Angulo *et al.*, 2006). However, according to Martin (2003) the Salvador-Bahia, northeastern Brazil (Fig. 1a), RSL curve shows the existence of two distinctive high-frequency oscillations at 4300-3500 cal yr BP and 2700-2100 cal yr BP. In addition, the interval between 5900 and 5300 cal yr BP was characterized by a rapid rise followed by an equally rapid fall. A RSL curve, based on 25 sea level

superficial indicators, dominantly of a biological nature (vermetid, mollusk shells and paleomangrove deposits) for the states of Pernambuco and Paraíba, northeastern Brazil (Fig. 1a, sector D), indicates that the RSL attained the present level at ~7400 cal yr BP, and its peak 2 – 3 m above the present level between 5000 – 4000 cal yr BP. The RSL has dropped since then to the present position. Minor RSL oscillations could have occurred from 3400 – 2100 to 600 cal yr BP (Suguio *et al.*, 2013). However, Angulo et al. (2006) disagree with that high-frequency RSL oscillations from the States of Bahia, northeastern Brazil, to Santa Catarina, southern Brazil, over the last 5000 years proposed by Suguio et al. (1985), due to lack of precision in time and space of some geological, biological and pre-historical records.

Regarding the Rio Grande do Norte, northeastern Brazil (Fig. 1a), the RSL approached its present position around 6500 cal yr BP (Bezerra et al., 2003 - fig. 1a sector B) and 6700 cal yr BP (Caldas et al., 2006 – fig. 1a, sector C), and it reached a highstand of 1.3 m at 5900 cal yr BP and subsequent drop to present values (Caldas *et al.*, 2006). According to Boski *et al.*, 2015 (Fig. 1a, sector D) a rapid RSL rise occurred between 8300 and 7000 cal yr BP in Rio Grande do Norte. Since then, the pace of RSL rise slowed and non-eustatic factors, namely terrigenous sediment supply and coastal dynamics, became dominant in the evolution of the estuary. Along the northern Brazilian littoral, the RSL stabilized at its current level between 7000 and 5000 yr BP (Behling and da Costa, 2000; Cohen et al., 2005 - fig. 1a, sector A).

Then, the Rio Grande do Norte littoral, northeastern Brazilian, should present a Holocene RSL changes between the maximum RSL (+5 m) of the southeastern Brazil (e.g. Angulo *et al.*, 2006) and the stable RSL (0 m) of the northern Brazil (Cohen *et al.*, 2005b). Noteworthy is the fact that along the Rio Grande do Norte

littoral, with ~260 km of coastline, there are not yet evidences of impacts of the Holocene sea-level changes and climate changes on mangroves based on sedimentary features, palynology and δ^{13}C, δ^{15}N, C/N analysis.

In order to present the mangrove development along the estuary of the Ceará Mirim River, Rio Grande do Norte, according to RSL and climate changes (allogenic processes), as well as local sedimentary dynamics (autogenic processes), a model of mangrove evolution is proposed based on sedimentary features, pollen content and δ^{13}C, δ^{15}N, C/N of sedimentary organic matter obtained of four sediment cores sampled from tidal flats occupied by mangroves and herbaceous vegetation.

Study area

The study sites are located at the mouth of the Ceará Mirim River (Fig. 1a). The fluvial course flows on crystalline rocks of the Seridó and Caicó Complexes and plutonic rocks, correlated to the Pre-Cambrian. These basement rocks are covered by Cretaceous units, Neogene and Quaternary deposits (Nogueira et al., 2010). At about 90 km north of the Ceará Mirim River, dune fields occur toward the hinterland. The young dunes and beaches occupy close to the shore and are moving subjected to permanent organization according to wind and wave direction, respectively (Caldas *et al.*, 2006).

The stretch of sampling sites is influenced by saline and dynamic tides and presents some tidal channels within the mangrove forest. Coastal plateau and coastal plain represent the main geomorphological features in the study area (Fig. 1b). The coastal plateau is represented by the Barreiras Formation (Miocene) that presents an abrupt contact with the coastal plain through a line of active and inactive cliffs. The Ceará Mirim river crosses the coastal plain causing a transition zone

under marine and fluvial influence, which is dominated by sand-clay and silty sediments. (Pfaltzgraff, 2010).

Natal, the Capital of the Rio Grande do Norte and 10 km away from the study area, is characterized by a tropical wet and dry climate ("Aw" and "As" in Köppen`s classification), and has a mean annual temperature of about 26ºC. The temperatures are highest and lowest on average in September and January, at about 26.8 °C and 25.8 °C, respectively. The lowest temperature recorded in Natal was 15.4°C in August 1999, and the highest was 34°C in December 2006. Precipitation averages 1464 mm/year, concentrated between March and July. The driest month is October (~18 mm) (INMET - Instituto Nacional de Meteorologia, 2017).

The studied area is mainly covered by mangroves, *várzea* (fluvial floodplain occupied by trees subjected to annual freshwater inundations (Assis and Wittmann, 2011)), herbaceous vegetation and wooded steppe savannah, which forms a discontinuous herbaceous substrate with few shrubs (Salgado et al., 1981 - Fig. 1a).

Materials and methods

Remote Sensing

The cartographic base was obtained through SRTM images obtained in the Catalog of Images freely available June 2016 by Brazilian National Institute for Space Research - INPE, Landsat 5 satellite, year 2011 and the vector files the Geological Survey of Brazil (CPRM) through download of Geobank platform (2016). The interpretation was supported by Google Earth Pro images 2016 that have higher resolution than the Landsat imagens used for the spatial analysis. The processing

resources were made using the software Global Mapper 12, ArcGIS 10.1 and QGIS 5.6.

Field work and sample processing

The fieldwork was carry out during the dry season of November 2014, and four sediment cores were sampled (Fig. 1a). The cores NAT1 (3.3 m depth, 1.17 km distant from modern coastline), NAT4 (3.5 m depth, 2.93 km distant from coastline), NAT6 (2 m depth, 2.83 km distant from coastline) and NAT8 (3.5 m depth, 1,84 km distant from coastline). The cores were taken by a Russian Sampler from a tidal flat occupied by mangrove (NAT1, 4 and 8) and herbaceous vegetation (NAT6). Visual observation and photographic documentation were used to determine the main geo-botanical units. The geographical positions of cores were determined by Global Positioning System (GPS) using the SAD69 as reference datum.

Facies description

Following the methods of Walker (1992), facies analysis was undertaken, including description of color (Color, 2009), lithology, texture and structure. The sedimentary facies were codified following Miall (1978). The studied stratigraphic profile was divided into facies associations, whereby sedimentary units are used to define a particular sedimentary environment (Reading, 1996). The cores were X-rayed to identify the sedimentary structures. Bulk samples (0.5 g each) were selected at 5 cm intervals for grain size analysis at the Chemical Oceanography Laboratory of the Federal University of Pará (UFPA), using a laser particle-size analyzer (SHIMADZU

SALD 2201). Hydrogen peroxide (H2O2) was used to eliminate organic matter, while residual sediments were disaggregated by ultrasound. Calculation of grain-size distribution follows Wentworth (1922), with separation of sand (2-0.0625 μm), silt (62.5-3.9 μm) and clay (3.9-0.12 μm) fractions. Macroscopic analysis of surface sediments was also carried out, recording size, sorting and rounding of sandy sediments.

Pollen and spore analysis

Two hundred and forty-six 1-cm^3 samples were taken at 5 cm intervals through the cores NAT1 (66 samples), NAT4 (70 samples), NAT6 (40 samples) and NAT8 (70 samples) for pollen analysis. All samples were prepared using standard pollen analytical techniques, including acetolysis (Erdtman, 1960). Sample residues were mounted on slides in a glycerin gelatin medium. Pollen and spores were identified by comparison with reference collections of about 4000 Brazilian forest taxa and various pollen keys (Salgado-Labouriau, 1973; Absy, 1975; Markgraf and D'Antoni, 1978; Roubik and Moreno, 1991; Colinvaux *et al.*, 1999), and based on the reference collection of the Laboratory of Coastal Dynamics, Federal University of Pará, and the [14]C Laboratory of the Center for Nuclear Energy in Agriculture (CENA/USP).

Pollen and spore data were presented in pollen diagrams as percentages of the total terrestrial pollen sum. The taxa were grouped according to source: mangroves, trees and shrubs, palms, herbs and ferns. The software TILIA and TILIAGRAF were used for calculation and to plot the pollen diagram (Grimm, 1987). CONISS was used for cluster analysis of pollen taxa, permitting the zonation of the pollen diagram. CONISS is a program for stratigraphically constrained cluster analysis by incremental sum of squares. It has been used widely for unconstrained

analyses and has proved particularly satisfactory for pollen frequency data (Grimm, 1987).

Isotopic and elemental analysis

A total of 141 samples (50-60 mg) were collected at 5 cm (NAT8), 10 cm (NAT1 and NAT4) and 30 cm (NAT6) intervals along the studied sediment cores. Considering that isotopic analysis has the potential to identify changes in the sources of organic matter for each depositional environment (characterized by the sedimentary features), the sampling intervals for isotopic and elemental analysis may be specific for each core. Then, the sampling intervals depend on the degree of stratigraphic heterogeneity along a core, where the cores with the minor changes in the granulometry and sedimentary structures have a longer sampling interval.

Sediments were treated with 4% HCl to eliminate carbonate, washed with distilled water until the pH reached 6, dried at $50^{\circ}C$, and finally homogenized. The samples were analyzed for total organic carbon (TOC), total nitrogen (TN), ^{13}C and ^{15}N by isotope ratio mass spectrometry at the Stable Isotope Laboratory of the Center for Nuclear Energy in Agriculture (CENA/USP). The results were expressed as a percentage of dry weight, with analytical precision of 0.09% (TOC) and 0.07% (TN), and as $\delta^{13}C$ and $\delta^{15}N$ expressed in per mil (‰) with respect to the VPDB and N_2 standards, respectively, with a precision of 0.2‰. Elemental results were used to calculate the C/N (weight/weight) for all samples. The determination of organic matter source, such as C_3 and C_4 terrestrial plants and/or marine and freshwater algae, will be environmental-dependent with a specific $\delta^{13}C$, $\delta^{15}N$ and C/N composition (Deines, 1980; Lamb et al., 2006; Meyers, 1997; Thornton and McManus, 1994).

Radiocarbon dating

Based on color, lithology and/or texture discontinuities, seven bulk samples (10 g each) were selected for radiocarbon analysis. In order to avoid natural contamination by shell fragments, roots, seeds, etc. sediment samples were physically cleaned under the stereomicroscope. Organic matter was extracted from the sampled material according to the laboratory standard pre-treatment in order to remove organic acids which are potential sources of young carbon contaminants to the samples (Pessenda et al., 2012). This treatment consisted of extracting residual material with 2-4% HCl at 60-80°C during 4 h, followed by a rinse with distilled water to neutralize the pH. The samples were dried at 50 ºC. A detailed description of the chemical treatment for sediment samples can be found in Pessenda et al. (2012).

A chronologic framework for the sedimentary sequence was provided by an accelerator-mass-spectrometer (AMS) dating at UGAMS (University of Georgia – Center for Applied Isotope Studies). Radiocarbon ages were normalized to a $\delta^{13}C$ value of -25‰ VPDB and reported as calibrated years (cal yr BP, 2σ) using CALIB 7.1 and the SHCal13 curve (Stuiver et al., 2017). The dates are reported in the text as the median of the range of calibrated ages (Table 1).

Results

Morphological settings and Vegetation

The study site extends by 7 km from the hinterland of valley Ceará Mirim River to current coastline (Fig. 1a). The Ceará Mirim River, which born in the Coastal Plateau, presents NW-SE direction and flows on Coastal Plain into the Atlantic Ocean. It exhibits a topographic difference between the floodplains and the plateau of about ~90 m. A striking characteristic of the Ceará Mirim river is its modern

channel pattern, which is mostly straight to only slightly sinuous. The mouth of the Ceará Mirim River crosses the coastal plain with floodplains presenting elevations of ~1.8 m above the mean sea-level. River discharge increases down the fluvial system producing a "straight" channel pattern. Currently, some small tidal channel was rectified due to shrimp farming activities (Fig. 1a). Shrimp farming occupies area ~2,8 Km^2 and cause the strongest impact on the vegetation together with surrounding urban occupation (Fig. 1a). Noteworthy is the presence of beachrocks on inshore surf zone; which are sedimentary rocks originated by the cementation of beach sediments by calcium carbonate, mostly calcite and/or aragonite in beach zone (Fig. 1a).

Regarding the modern vegetation, the coastal plain of the Ceará Mirim River is characterized by fresh and brackish water vegetation. Mangroves cover ~4.8 Km^2 of the study area and are mainly characterized by *Rhizophora mangle* and *Avicennia germinans*, which are currently restricted to the estuary and 5 km along the fluvial valley (Fig. 1a). They are occurring along tidal channels, within specific topographic zones with a presence of *Avicennia* at highest elevations above mean spring tide level, while the *Rhizophora* occupies topographically lower zones upriver.

Herbaceous vegetation (4.6 Km^2) occurs on highest sector of the tidal flats, mainly represented by *Poaceae, Cyperaceae, Borreria* and some *Arecaceae* (Fig. 1a). However, some herbs occupy also low topographic levels, colonizing river banks and estuarine tidal flats.

Upstream, sandy silt and muddy sediments spread over the fluvial plain mainly dominated by "várzea" vegetation, which covers 6,9 km^2 (swampland seasonally and permanently inundated by freshwater). The limit between freshwater and mangrove vegetation is not always clearly fixed, because the transition between

these vegetation units respond to a salinity gradient, where the vegetation, mainly characterized by *Arecaceae* (freshwater vegetation), is positioned upstream, while mangroves occupy zones under marine influence. In addition, the coastal plain presents areas with some species of *várzea* and savanna that characterizes the transition forest. On the coastal plateau occurs wooded steppe savannah that forms a discontinuous herbaceous substrate, mainly formed by *Cyperaceae* and *Poaecea*, with few shrubs mainly represented by *Anacardiaceae* and *Malpighiaceae* (Fig. 1a).

Radiocarbon dates and sedimentation rates

The radiocarbon dates are shown in Table 1. No age inversions were observed. Estimated sedimentary rates are 4.6 mm/yr (330 - 170 cm) and 0.93 mm/yr (170 - 0 cm) core NAT1 (Fig. 8). The NAT4 presents rates of 12 mm/yr (320 - 200 cm), 0.25 mm/yr (200 - 105 cm) and 0.93 mm/yr (105-0 cm) (Fig. 6). The NAT6 and NAT8 revealed sedimentation rates of 0.25 mm/yr (178 – 0 cm) and 0.48 mm/yr (270-0 cm), respectively (Figs 4 and 2). These rates are in the same order of magnitude than the vertical accretion interval of 0.1 and 11 mm yrs^{-1} from mangrove forests from northern Brazilian littoral and Florida-USA reported by other authors (Cahoon and Lynch, 1997; Behling *et al*., 2004; Vedel *et al.*, 2006; Cohen *et al*., 2009; Guimarães *et al*., 2010).

Facies description

The studied cores record sedimentary successions represented mainly by massive sand and heterolithic deposits (Figs. 2, 4, 6, and 8). The integration of sedimentary facies, pollen data and geochemical records allowed to define three facies associations: (A) Tidal channel, (B) Mangrove tidal flat and (C) Herbs/mangrove mixed tidal flat (Table 2).

Facies association A (Tidal Channel)

This facies association (A) occurs along the intervals 355-270 cm, 250-125 cm (NAT8), 350 -280 cm, 100-55 cm (NAT4), 330-200 cm (NAT1) and 200-175 cm (NAT6) (Figs. 2, 4, 6 and 8). It consists of several fining upward successions of massive sand, cross-stratified, cross-laminated and flaser heterolithic bedding. Massive sands with shells are present only in cores NAT4 and NAT8 (Figs. 2 and 6).

The pollen assemblages of association A, where 36 pollen taxa were identified, are dominated by trees and shrubs pollen (0-67%) characterized mostly by Rubiaceae (5-45%), Euphorbiaceae (3-36%), Mimosaceae (0-23%), *Psychotria* (0-17%), Malpighiaceae (0-8%), Aizoaceae (0-8%) and Myrtaceae (0-7%). The mangrove pollen (0-65%) are mainly constituted by *Rhizophora* (5-57%) and *Avicennia* (0-3%). The palms ecological group appear with very low percentages (<10%). The herb pollen (0-58%) are represented by Poaceae (0–47%), Cyperaceae (0-21%) and *Borreria* (0-14%) (Figs. 3, 5, 7 and 9). The intervals between 355 and 270 cm, and 200 and 155 of the cores NAT8 and NAT6, respectively (Fig. 3 and 5), are characterized by absence of pollen, probably due to increase of sandy sediments (Havinga, 1967).

The $\delta^{13}C$ and $\delta^{15}N$ values are between -27 and ~-19‰ (mean 23.2‰) and 0.68 and 5.2‰ (mean 2.9‰), respectively. TOC and TN present values between 0.9 and 15.5% (mean 8,2%) and 0.03 to 0.4% (mean 2.2%), respectively. The C/N values occurs between 2 and 115 (Figs. 2, 4, 6 and 8).

Facies Association B (Mangrove Tidal flat)

It occurs between 135 and 0 cm (NAT6), 280 and 100 cm, 55 and 0 cm (NAT4) and 200 and 0 cm (NAT1) (Figs. 2, 4, 6 and 8). It is mainly characterized by wavy heterolithic bedding (Fig. 2).

This facies association presents mainly mangrove pollen (0-76%) represented by *Rhizophora* (0-86%) and *Avicennia* (0-14%). The pollen spectra include also ecological groups of trees and shrubs (0-64%) composed mainly by Rubiaceae (3-25%), Fabaceae (2-16%), Mimosaceae (0-18%), Euphorbiaceae (2-10%), Malpighiaceae (0-11%), Myrtaceae (0-7%), Burseraceae (0-8%) and Amaranthaceae (0-6%). Herbs group (0-74%) are mainly characterized by Poaceae (0–48%), Cyperaceae (8–42%), *Asteraceae* (0-24%) and *Borreria* (0-18%). Arecaceae pollen (0-12%) are also present along this facies association. Ferns (0-11%) are represented by trilete and monolete psilate (Figs. 3, 5, 7 and 9).

The $\delta^{13}C$ and $\delta^{15}N$ values are between -27‰ and -24.3‰ (mean -26‰) and 0.26 and 6.19‰ (mean 3.22‰). The TOC and TN exhibit values between 0.74 and 15.52% (mean 8.13%) and 0.02 and 0.72 % (mean 0.37%). The C/N values occur between 14 and 68 (Figs. 2, 4, 6 and 8).

Facie Association C (Herbs/mangrove mixed tidal flat)

It may be recognized along the intervals 180-135 cm in the core NAT 6 and 260-245 cm and 125-0 cm in the NAT8 (Figs. 2 and 4). This facies association consists of heterolithic lenticular bedding with bioturbation features such as woody roots, root marks and dwelling structures produced by the benthic fauna. Along the interval 125-65 cm in the NAT8 shells are present (Fig. 2). According to the pollen analysis, taxa representative of trees and shrubs (0-65%) dominate the pollen

assemblage, and it is mainly composed by Mimosaceae (0-45%), Fabaceae (0-20%), Euphorbiaceae (0-15%), Malpighiaceae (0-18%) and Anacardiaceae (0-7%). Herb pollen (0-69%) are composed by Poaceae (0-57%), Cyperaceae (0-17%), Asteraceae (0-10%) and *Borreria* (0-4%). Mangrove pollen (0-43%) are represented only by *Rhizophora* (0-3%). Palms (0-6%) occurs with low percentage (Figs. 7 and 9). Pollen grains was not identified along the interval 125 - 65 cm in core NAT6 (Fig. 5). Some intervals with absence of pollen or only a few pollen grains (<3000 grains/cm3) have been related mainly to sediment grain size, microbial attack and oxidation. In addition, it may be due to characteristics inherent to the pollen grains, such as sporopollenine content, as well as the chemical and physical composition of the pollen wall (Havinga, 1967). Pollen grains tend to deteriorate rapidly in sandy sediments when compared to muddy deposits due to the better drainage of sands caused by large interstitial pores, which allows the pollen grains to be abraded by mobile inorganic matrix and oxidized during soil hydration-dehydration cycles (Faegri, 1971; Grindrod, 1988).

The organic geochemical data reveal values for $\delta^{13}C$ and $\delta^{15}N$ between -27.5 and 26.4‰ (mean -26.9‰), and 0.02 and 8.1‰ (mean 4.6‰), respectively. The TOC and TN values occur between 3 and 14% (mean 8.5%) and 0.01 and 0.13% (mean 0.28%), respectively. The C/N exhibits values between 32 and 37 (Figs. 6 and 8).

Interpretation and discussions

Based on sedimentary features, the fining-upward facies successions with shells followed by mud accumulation, recorded in the cores NAT8, NAT6 and NAT4 (Figs. 2, 4 and 6) reveal a tidal channel filling process according to its lateral migration. This process involves point-bar lateral accretion within a meandering

channel draining intertidal mudflats, where periodic fluctuations of current velocity/direction and water levels inherent to the tidal cycles, allowed sand and mud deposition during periods of high (ebb or flood tidal current) and low (slack water) energy flows, respectively (Thomas et al., 1987).

This tidal channel dynamics built up an upward-fining succession, with thick sand deposition succession at the base, including subtidal channel-filling, topped by intertidal muddy deposits. This intertidal flat comprises sediments with well-developed wavy heterolithic bedding at the base and lenticular bedding at the top, overlapped by wetland deposits. The intertidal flats with mangroves are generally bordered by estuarine/tidal channels in a sheltered coastal environment.

Pollen, δ^{13}C and C/N data provide evidences that estuarine organic matter and C3 terrestrial plants accumulated during the mangrove phase (Fig. 11). Mangroves, herbs and palms occupied tidal flats on margin of an estuarine/tidal channel, while the trees and shrubs occupied the plateau (Figs. 1b and 12). The relatively high percentages (20-40%) of trees and shrubs pollen may be associated to the elevated pollen inflow of trees and shrubs (Atlantic Forest) from this plateau.

Palynological evidence for the presence of mangrove vegetation, together with micro-foraminifera (Kumaran et al., 2004), indicate an estuarine influence since ~6920 cal yr BP. The finning upward cycles with heterolithic bedding and mangrove pollen suggests distinct phases of establishment, expansion and loss of mangrove area according to the tidal channels dynamics. The tidal channels activity is the product of the interaction between the river discharge and tidal waves eroding and filling the coastal depressions. The tidal-fluvial channel shows high lateral migration, typical of low-gradient rivers with elevated suspension load (Schumm, 1977). Then,

this process has formed and destroyed the substrate suitable for mangrove development during the middle and late Holocene (Fig. 12).

In this context, it should be noted that tidal currents in mangrove forests are impeded by the friction caused by the high mangrove vegetation density. The sediment particles carried in suspension into the forest during tidal inundation are cohesive, mainly clay and fine silt, and form large flocs. These flocs remain in suspension because of the turbulence created by the flow around the vegetation. The intensity of sedimentation is largest for trees forming a complex matrix of roots such as *Rhizophora*. The flocs settle in the forest mainly around slack high tide. Hence the inundation of coastal mangrove forests works as a pump preferentially transporting fine, cohesive sediment from coastal and fluvial waters to mangroves. Then, mangroves are contributing to the creation of mud banks and this process makes the mangrove forests an important sink for suspended sediment (Furukawa and Wolanski, 1996). Therefore, mangroves tend to mitigate the erosion caused by storms and RSL rise (Gedan et al., 2011).

Considering this process, the flood plains, occupied by herbaceous vegetation along upstream of the Ceará Mirim River and positioned topographically higher than modern mangrove tidal flats, present predominance of sandy sediments. The absence of remaining organic mud sediments on flood plains may indicate that mangroves have not development above the limit of the modern tidal range, upstream of the Ceará Mirim River. It suggests that RSL during the Holocene never has been above the modern RSL on study area. Should be highlighted that lateral migration of the coast line depends on the balance between sedimentary supply, in this case mainly from the Ceará Mirim River, and the available accommodation space, controlled by the RSL, in a certain timespan. Then, a marine regression can

occur when sufficient sediment is entering into the coastal system to overcome the amount of space available. This can occur during stillstands or RSL rises, and is referred as a "normal" regression. In this case, the mudflat may be no longer affected by brackish water, and, consequently the mangroves migrate to a lower topographic position. When no sediment is delivered to the shoreline during a RSL fall, the regression is said to be forced because a seaward shift of the shoreline must occur, even if the volume of sediment supplied is low (Posamentier et al., 1992).

Some studies indicate that RSL in Rio Grande do Norte approached its present position between 6500 and 6700 cal yr BP, and it reached a highstand of 1.3 m at 5900 cal yr BP and subsequent drop to present values (Bezerra et al., 2003; Caldas et al., 2006). According to Boski et al. (2015) a rapid RSL rise occurred between 8300 and 7000 cal yr BP in Rio Grande do Norte. After that, processes associated with terrigenous sediment supply and coastal dynamics dominated the evolution of the estuary. Along the northern Brazilian littoral, the RSL stabilized at its current level between 7000 and 5000 yr BP (Behling and da Costa, 2000; Cohen et al., 2005).

Considering a RSL higher than the modern one and a stable fluvial discharge during the middle Holocene, mangroves would have expanded on flood plains and accumulated organic mud banks in higher topographic zones above the modern tidal range. Such a situation was recorded in a floodplain of the Jucuruçu River, near the city of Prado-Bahia, northeastern Brazil, 23 km distant from the coastline, where a stratigraphic succession revealed the presence of an estuarine system with tidal flats colonized by mangroves and sedimentary organic matter sourced from estuarine organic matter 3.4 ± 1.35 m above the modern mangrove zone during the middle Holocene (Fontes et al., 2017).

The cores from the Ceará Mirim River present muddy deposits with mangrove pollen only within the modern tidal range during the last ~7000 cal yr BP (Fig. 10). Therefore, based on these data, after the post-glacial sea-level rise, the RSL has reached the modern level at about 7000 cal yr BP, and it has been stable or with possible small oscillations (<~1m) since then. This analysis considers the vertical range of substrates occupied by mangroves. For instance, along the northern Brazilian littoral mangroves may occur within a topographic range of up to 1.5 m. Obviously, the lower mangrove limits are positioned near coastline, and the higher boundaries occur upstream. These topographic limits depend mainly on the interaction between fluvial discharge and tidal range (Cohen et al., 2012, 2005; Cohen and Lara, 2003; Lara and Cohen, 2006).

Regarding climate changes, Prado et al. (2013) proposed an early to mid-Holocene water deficit scenario in eastern South America compared to the late Holocene. Studies in Brazil indicate a relatively drier period during the early Holocene, while the middle to late Holocene climate was marked by wetter conditions (Barberi et al., 2000; Ferraz-vicentini and Salgado-Labouriau, 1996; Ledru, 1993; Pessenda et al., 2004). Therefore, changes in rainfall regime (Absy, 1991; Freitas et al., 2001; Molodkov and Bolikhovskaya, 2002) caused changes in fluvial discharge and estuarine salinity gradients (Lara and Cohen, 2006).

Along the studied cores occur muddy layers with mangrove pollen. It suggests a tidal water salinity suitable to the mangrove development during the last ~7000 cal yr BP. Then, the fluvial discharge has not changed significantly to cause a hypersaline tidal flat or freshwater floodplain, considering a lower or higher river discharge, respectively. Both situations are inadequate to mangrove development. Mangroves occur naturally along salinity gradients from 10 to 90‰. In northern

Brazilian mangrove, this system includes different vegetation types ranging from low-salinity, high *Rhizophora* forests to hypersaline environments with an *Avicennia* dwarf forest, to a salt marsh with succulent plants (Cohen and Lara, 2003).

Based on relation mangrove/freshwater vegetation pollen, isotope and sedimentary features Cohen et al. (2012) propose that the Amazonian mangrove belt was formed by a marine incursion caused by post-glacial sea-level rise during the early and middle Holocene. The fragmentation of this continuous mangrove line during the late Holocene was caused likely by the increase of river freshwater discharge associated to the change from dry into wet climates in the late Holocene when the mangroves were replaced by freshwater vegetation.

Considering the present study, based on the stratigraphic successions, modern vegetation and geomorphology, no evidence indicating significate sea level and climate changes since ~7000 cal yr BP have been recorded along the Ceará Mirim River. We would like to emphasize that this does not mean that there were absolutely no climate changes and RSL fluctuations at the study site during the Holocene. Eventually, some signal of influence of the sea-level (<~1 m) and climate changes on mangrove dynamics in this estuarine channel must have been weakened by more intense activity of tidal channels (Fig. 12).

Therefore, this work proposes an autogenic process controlling the mangrove dynamics over the last 7000 cal yr BP along the Ceará Mirim River. Autogenic processes are intrinsic to the depositional system (Cecil, 2013), involving the redistribution of energy and materials within a sedimentary system, and are of limited occurrence in time. They are related to the action of tides and storms, channel avulsion, delta switching, lateral migration of meandering fluvial point-bars and beach-barrier bars, etc. (Beebower, 1964).

Along the studied cores, an autogenic process may be recognized by a facies succession such as inclined heterolithic stratification (HIS), cross stratified sand (Scs) and massive sand (Sm) followed by flaser, wave and lenticular heterolithic bedding (Hw) that reveal an active channel and its abandonment caused by lateral migration of channels (Reineck and Wunderlich, 1968) (Figs. 2, 4, 6 and 8). Noteworthy is the fact that muddy tidal flats formed after the channel abandonment provide suitable conditions for pollen preservation sourced from vegetation surrounding the sedimentary environment from the time that sediment was deposited (Cohen et al., 2008), reflecting the plants colonizing the study site.

Then, not all vegetation changes may be attributed to allogenic process, such as relative sea-level and climate changes. Autogenic processes affect the depositional environments and consequently the wetlands zone on tidal/fluvial plains in a local and short time scale. An example of autogenic process controlling the palaeoflora was presented by Moraes et al. (2017), where the authors proposes allogenic process as the main driving forces controlling the wetlands dynamics along the Jucuruçu River-Bahia, northeastern Brazil during the Holocene. However, his work also reveals that part of the changes in vegetation over the last ~700 years reflects tidal channels and tidal flats development, which represent autogenic process. Therefore, the change of time scale analysis from the Holocene to the last centuries has weakened the influence of allogenic factors. However, this time scale analysis should be correlated with the dimensions of depositional environment, where the larger the depositional system analyzed, the stronger the influence of autogenic processes on stratigraphic sequences during a longer time scale.

This analysis is essential to distinguish the effects of climate changes for the next decades (Marengo, 2006) and the sea level rise between 1.8 and 2.4 mm/yr for

until the end of this century (Church et al., 2013) from the autogenic processes on mangroves.

Conclusions

The present investigation combining sedimentary features, pollen and isotopes data from four sediment cores, as well as geomorphological and vegetation analyses based on remote sensing revealed an estuarine influence with mangrove development along the Ceará Mirim River, Northeastern Brazil, since ~6920 cal yr BP after the post-glacial sea level rise, and it has been stable during the middle and late Holocene. The mangrove expansion along this fluvial valley since the middle Holocene was caused by the sea-level stabilization. However, sedimentary sequences formed by sandy deposits and heterolithic beddings are correlated with the absence and presence of mangrove vegetation, respectively, suggesting a wetland dynamic mainly controlled by autogenic factors, relating to tidal channel migrations, instead of allogenic process, associated with sea level and/or climate change, over the last ~6920 cal yr BP. Some influence of sea-level and climate changes on mangrove dynamics in this estuarine channel have been weakened by more intense tidal channels activities.

This study provides elements to discern, along a stratigraphic record, allogenic and autogenic influence on depositional environment occupied by mangroves. The mangrove dynamics in face of climate changes and RSL rise in a decadal and secular range is a new challenging question, because mechanisms related to the natural dynamics of depositional environments, such as channel migration, littoral drift currents, tidal and waves action have strong influences on the establishment and degradation of mangroves. Then, it is crucial identify the effects of autogenic processes on mangrove dynamics, otherwise impacts on mangroves

caused by autogenic processes may be erroneously attributed to climate and sea-level changes.

Acknowledgments

References

Absy, M.L., 1975. Polen e esporos do Quaternário de Santos (Brasil). Hoehnea 5, 1–26.

Absy, M.L., 1991. Mise en evidence de quatre phases d'ouverture de la foret dense dans le sud-est de l'Amazonie au cours des 60 000 dernieres annees. Premiere comparaison avec d'autres regions tropicales. Comptes Rendus - Acad. des Sci. Ser. II.

Angulo, R., Lessa, G., Souza, M., 2006. A critical review of mid- to late-Holocene sea-level fluctuations on the eastern Brazilian coastline. Quat. Sci. Rev. 25, 486–506.

Angulo, R.J., Lessa, G.C., Souza, M.C. De, 2006. A critical review of mid- to late-Holocene sea-level fluctuations on the eastern Brazilian coastline. Quat. Sci. Rev. 25, 486–506.

Assis, R.L. de, Wittmann, F., 2011. Forest structure and tree species composition of the understory of two central Amazonian várzea forests of contrasting flood heights. Flora - Morphol. Distrib. Funct. Ecol. Plants 206, 251–260.

Barberi, M., Salgado-Labouriau, M.L., Suguio, K., 2000. Paleovegetation and paleoclimate of "Vereda de Águas Emendadas", central Brazil. J. South Am. Earth Sci. 13, 241–254.

Beebower, J.R., 1964. Cyclothems and cyclic depositional mechanism in alluvial plain sedimentation. Bull. Kans. Univ. Geol. Surv. 169, 35–42.

Behling, H., Cohen, M.L., Lara, R., 2004. Late Holocene mangrove dynamics of Marajó Island in Amazonia, northern Brazil. Veg. Hist. Archaeobot. 13, 73–80.

Behling, H., da Costa, M.L., 2000. Holocene Environmental Changes from the Rio Curuá Record in the Caxiuanã Region, Eastern Amazon Basin. Quat. Res. 53, 369–377.

Bezerra, F.H.., Barreto, A.M.., Suguio, K., 2003. Holocene sea-level history on the Rio Grande do Norte State coast, Brazil. Mar. Geol. 196, 73–89.

Boski, T., Bezerra, F.H.R., de Fátima Pereira, L., Souza, A.M., Maia, R.P., Lima-Filho, F.P., 2015. Sea-level rise since 8.2ka recorded in the sediments of the Potengi–Jundiai Estuary, NE Brasil. Mar. Geol. 365, 1–13.

Cahoon, D.R., Lynch, J.C., 1997. Vertical accretion and shallow subsidence in a mangrove forest of southwestern Florida, U.S.A. Mangroves Salt Marshes 1, 173–186.

Caldas, L.H. de O., Oliveira, J.G. de, Medeiros, W.E. de, Stattegger, K., Vital, H., 2006. Geometry and evolution of Holocene transgressive and regressive barriers on the semi-arid coast of NE Brazil. Geo-Marine Lett. 26, 249–263.

Castro, D.F., Rossetti, D.F., Cohen, M.C.L., Pessenda, L.C.R., Lorente, F.L., 2013. The growth of the Doce River Delta in northeastern Brazil indicated by sedimentary facies and diatoms. Diatom Res. 28, 455–466.

Cecil, C.B., 2013. An overview and interpretation of autocyclic and allocyclic processes and the accumulation of strata during the Pennsylvanian–Permian transition in the central Appalachian Basin, USA. Int. J. Coal Geol. 119, 21–31.

Church, J.A., Clark, P.U., Cazenave, A., Gregory, J.M., Jevrejeva, S., Levermann, A., Merrifield, M.A., Milne, G.A., Nerem, R.S., Nunn, P.D., Payne, A.J., Pfeffer, W.T., Stammer, D., Unnikrishnam, A.S., 2013. Sea level change, in: Stocker, T.F., Qin, D., Plattner, G.-K., Tignor, M., Allen, S.K., Boschung, J., Nauels, A., Xia, Y., Bex, V., Midgley, P.M. (Eds.), Climate Change 2013: The Physical Basis, Contribution of Working Group I to the Fifth Assessment Report of the

Intergovernmental Panel on Climate Change. Cambridge, pp. 1029–1136.

Cohen, M.C.L., Behling, H., Lara, R.J., 2005. Amazonian mangrove dynamics during the last millennium : The relative sea-level and the Little Ice Age 136, 93–108.

Cohen, M.C.L., Behling, H., Lara, R.J., Smith, C.B., Matos, H.R.S., Vedel, V., 2009. Impact of sea-level and climatic changes on the Amazon coastal wetlands during the late Holocene. Veg. Hist. Archaeobot. 18, 425–439.

Cohen, M.C.L., Fran??a, M.C., de F??tima Rossetti, D., Pessenda, L.C.R., Giannini, P.C.F., Lorente, F.L., Junior, A. ??lvaro B., Castro, D., Macario, K., 2014. Landscape evolution during the late Quaternary at the Doce River mouth, Esp??rito Santo State, Southeastern Brazil. Palaeogeogr. Palaeoclimatol. Palaeoecol. 415, 48–58.

Cohen, M.C.L., França, M.C., Rossetti, D.F., Pessenda, L.C.R., Giannini, P.C.F., Lorente, F.L., Buso Junior, A.., Castro, D., Macario, K., 2014. Landscape evolution during the late Quaternary at the Doce River mouth, Espírito Santo State, Southeastern Brazil. Palaeogeogr. Palaeoclimatol. Palaeoecol. 415, 48–58.

Cohen, M.C.L., Lara, J., 2003. Temporal changes of mangrove vegetation boundaries in Amazonia : Application of GIS and remote sensing techniques 223–231.

Cohen, M.C.L., Lara, R.J., Smith, C.B., Angélica, R.S., Dias, B.S., Pequeno, T., 2008. Wetland dynamics of Marajó Island, northern Brazil, during the last 1000 years. CATENA 76, 70–77.

Cohen, M.C.L., Pessenda, L.C.R., Behling, H., de Fátima Rossetti, D., França, M.C., Guimarães, J.T.F., Friaes, Y., Smith, C.B., 2012. Holocene palaeoenvironmental history of the Amazonian mangrove belt. Quat. Sci. Rev. 55, 50–58.

Cohen, M.C.L., Souza Filho, P.W.M., Lara, R.J., Behling, H., Angulo, R.J., 2005. A model of Holocene mangrove development and relative sea-level changes on the Bragança Peninsula (northern Brazil). Wetl. Ecol. Manag. 13, 433–443.

Cohen, M.C.L., Souza Filho, P.W.M., Lara, R.J., Behling, H., Angulo, R.J., 2005. A Model of Holocene Mangrove Development and Relative Sea-level Changes on the Bragança Peninsula (Northern Brazil). Wetl. Ecol. Manag. 13, 433–443.

Colinvaux, P., De Oliveira, P.E., Patiño, J.E.M., 1999. Amazon Pollen Manual and Atlas. Harwood Academic Publishers, Dordrecht.

Color, M., 2009. Munsell Soil Color Charts, in: Munsell Soil Color Charts. New Windsor, NY.

Deines, P., 1980. The isotopic composition of reduced organic carbon, in: Fritz, P., Fontes, J.C. (Eds.), Handbook of Environmental Isotope Geochemistry. The Terrestrial Environments. Elsevier, Amsterdam, pp. 329–406.

Erdtman, G., 1960. The acetolysis method: in a revised description. Sven. Bot. Tidskr. Lund 54, 561–564.

Faegri, K., 1971. The preservation of sporopollenin membranes under natural conditions, in: Brooks, J., Grant, P.R., Muir, M., Gijzel, P.V., Shaw, G. (Eds.), Sporopollenin. Academic Press, London, New York, pp. 256–270.

Ferraz-vicentini, K.R., Salgado-Labouriau, M.L., 1996. Palynological analysis of a palm swamp in Central Brazil. J. South Am. Earth Sci. 9, 207–219.

Fontes, N.A., Moraes, C.A., Cohen, M.C.L., Alves, I.C.C., França, M.C., Pessenda, L.C.R., Francisquini, M.I., Bendassolli, J.A., Macario, K., Mayle, F., 2017. The Impacts of the Middle Holocene High Sea-Level Stand and Climatic Changes on Mangroves of the Jucuruçu River, Southern Bahia – Northeastern Brazil. Radiocarbon 59, 215–230.

França, M.C., Alves, I.C.C., Castro, D.F., Cohen, M.C.L., Rossetti, D.F., Pessenda, L.C.R., Lorente, F.L., Fontes, N.A., Junior, A.Á.B., Giannini, P.C.F., Francisquini, M.I., 2015. A multi-proxy evidence for the transition from estuarine mangroves to deltaic freshwater marshes, Southeastern Brazil, due to climatic and sea-level changes during the late Holocene. CATENA 128, 155–166.

França, M.C., Francisquini, M.I., Cohen, M.C.L., Pessenda, L.C.R., Rossetti, D.F., Guimarães, J.T.F., Smith, C.B., 2012. The last mangroves of Marajó Island — Eastern Amazon : Impact of climate and/or relative sea-level changes. Rev. Palaeobot. Palynol. 187, 50–65.

Freitas, H.A., Pessenda, L.C.R., Aravena, R., Gouveia, S.E.M., de Souza Ribeiro, A., Boulet, R., 2001. Late Quaternary Vegetation Dynamics in the Southern Amazon Basin Inferred from Carbon Isotopes in Soil Organic Matter. Quat. Res. 55, 39–46.

Furukawa, K., Wolanski, E., 1996. Sedimentation in Mangrove Forests. Mangroves Salt Marshes 1, 3–10.

Gedan, K.B., Kirwan, M.L., Wolanski, E., Barbier, E.B., Silliman, B.R., 2011. The present and future role of coastal wetland vegetation in protecting shorelines: Answering recent challenges to the paradigm. Clim. Change 106, 7–29.

Grimm, E.C., 1987. CONISS: a FORTRAN 77 program for stratigraphically constrained cluster analysis by the method of incremental sum of squares. Comput. Geosci. 13, 13–35.

Grindrod, J., 1988. The palynology of holocene mangrove and saltmarsh sediments, particularly in Northern Australia. Rev. Palaeobot. Palynol. 55, 229–245.

Guimarães, J.T.F., Cohen, M.C.L., França, M.C., Lara, R.J., Behling, H., 2010. Model of wetland development of the Amapá coast during the late Holocene. An. Acad. Bras. Cienc. 82, 451–465.

Guimarães, J.T.F., Cohen, M.C.L., Pessenda, L.C.R., Franca, M.C., Smith, C.B., Nogueira, A.C.R., 2012. Mid- and late-Holocene sedimentary process and palaeovegetation changes near the mouth of the Amazon River. The Holocene 22, 359–370.

Havinga, A.J., 1967. Palynology and pollen preservation. Rev. Paleobotany Palynol. 2, 81–98.

Kumaran, K.P.N., Shindikar, M., Limaye, R.B., 2004. Mangrove associated lignite beds of Malvan, Konkan: Evidence for higher sea-level during the Late Tertiary (Neogene) along the west coast of India. Curr. Sci. 86, 335–340.

Lamb, A.L., Wilson, G.P., Leng, M.J., 2006. A review of coastal palaeoclimate and relative sea-level reconstructions using δ13C and C/N ratios in organic material. Earth-Science Rev. 75, 29–57.

Lara, R.J., Cohen, M.C.L., 2006. Sediment porewater salinity, inundation frequency and mangrove vegetation height in Bragança, North Brazil: an ecohydrology-based empirical model. Wetl. Ecol. Manag. 14, 349–358.

Lara, R.J., Cohen, M.C.L., 2009. Palaeolimnological studies and ancient maps confirm secular climate fluctuations in Amazonia. Clim. Change 94, 399–408.

Ledru, M.-P., 1993. Late Quaternary Environmental and Climatic Changes in Central Brazil. Quat. Res. 39, 90–98.

Lorente, F.L., Pessenda, L.C.R., Oboh-Ikuenobe, F., Buso Jr., A.A., Cohen, M.C.L., Meyer, K.E.B., Giannini, P.C.F., de Oliveira, P.E., Rossetti, D. de F., Borotti Filho, M.A., França, M.C., de Castro, D.F., Bendassolli, J.A., Macario, K., 2013. Palynofacies and stable C and N isotopes of Holocene sediments from Lake Macuco (Linhares, Espírito Santo, southeastern Brazil): Depositional settings

and palaeonvironmental evolution. Palaeogeogr. Palaeoclimatol. Palaeoecol. 55, 325–330.

Lorente, F.L., Pessenda, L.C.R., Oboh-Ikuenobe, F., Buso Jr., A.A., Cohen, M.C.L., Meyer, K.E.B., Giannini, P.C.F., de Oliveira, P.E., Rossetti, D.F., Borotti Filho, M.A., França, M.C., de Castro, D.F., Bendassolli, J.A., Macario, K., 2014. Palynofacies and stable C and N isotopes of Holocene sediments from Lake Macuco (Linhares, Espírito Santo, southeastern Brazil): Depositional settings and palaeoenvironmental evolution. Palaeogeogr. Palaeoclimatol. Palaeoecol. 415.

Marengo, J.A., 2006. Mudanças climáticas globais e seus efeitos sobre a biodiversidade: caracterização do clima atual e definição das alterações climáticas para o território brasileiro ao longo do século XXI. Ministério do Meio Ambiente, Brasilia.

Markgraf, V., D'Antoni, H.L., 1978. Pollen Flora of Argentina. University of Arizona Press, Tucson.

Martin, L., Dominguez, J.M.L., Bittencourt, A.C.S.P., 2003. Fluctuating Holocene Sea Levels in Eastern and Southeastern Brazil: Evidence from Multiple Fossil and Geometric Indicators. J. Coast. Res. 19, 101–124.

Meyers, P.A., 1997. Organic geochemical proxies of paleoceanographic, paleolimnologic, and paleoclimatic processes. Org. Geochem. 27, 213–250.

Miall, A.D., 1978. Facies types and vertical profile models in braided river deposits: a summary, in: Miall, A.D. (Ed.), Fluvial Sedimentology. Canadian Society of Petroleum Geologists, Calgary, p. 597–604.

Molodkov, A.N., Bolikhovskaya, N.S., 2002. Eustatic sea-level and climate changes over the last 600 ka as derived from mollusc-based ESR-chronostratigraphy and pollen evidence in Northern Eurasia. Sediment. Geol. 150, 185–201.

Moraes, C.A., Fontes, N.A., Cohen, M.C.L., Fran?a, M.C., Pessenda, L.C.R., Rossetti, D.F., Francisquini, M.I., Bendassolli, J.A., Macario, K., 2017. Late Holocene mangrove dynamics dominated by autogenic processes. Earth Surf. Process. Landforms.

Nogueira, F.C., Bezerra, F.H.R., Fuck, R.A., 2010. Quaternary fault kinematics and chronology in intraplate northeastern Brazil 49, 79–91.

Pessenda, L.C.R., Ribeiro, A.D.S., Gouveia, S.E.M., Aravena, R., Boulet, R., Bendassolli, J.A., 2004. Vegetation dynamics during the late Pleistocene in the Barreirinhas region, Maranhão State, northeastern Brazil, based on carbon isotopes in soil organic matter. Quat. Res. 62, 183–193.

Pessenda, L.C.R., Vidotto, E., De Oliveira, P.E., Buso, A.A., Cohen, M.C.L., Rossetti, D. de F., Ricardi-Branco, F., Bendassolli, J.A., 2012. Late Quaternary vegetation and coastal environmental changes at Ilha do Cardoso mangrove, southeastern Brazil. Palaeogeogr. Palaeoclimatol. Palaeoecol. 363, 57–68.

Pfaltzgraff, P.A. dos S., 2010. Geodiversidade do estado do Rio Grande do Norte. Recife.

Posamentier, H.W., Allen, G.P., James, D.P., Tesson, M., 1992. Forced regressions in a sequence stratigraphic framework: Concepts, examples, and exploration significance. Am. Assoc. Pet. Geol. Bull. 76, 1687–1709.

Prado, L.F., Wainer, I., Chiessi, C.M., Ledru, M.-P., Turcq, B., 2013. A mid-Holocene climate reconstruction for eastern South America. Clim. Past 9, 2117–2133.

Reading, H.G., 1996. Sedimentary Environments: Processes, Facies and Stratigraphy, 3a ed. Blackwell Science.

Reineck, H.E., Wunderlich, F., 1968. Classification and origin of flaser and lenticular

bedding. Sedimentology 11, 99–104.

Rossetti, D. de F., Polizel, S.P., Cohen, M.C.L., Pessenda, L.C.R., 2015. Late Pleistocene–Holocene evolution of the Doce River delta, southeastern Brazil: Implications for the understanding of wave-influenced deltas. Mar. Geol. 367, 171–190.

Roubik, D.W., Moreno, J.E., 1991. Pollen and Spores of Barro Colorado Island. Missouri Botanical Garden.

Salgado-Labouriau, M.L., 1973. Contribuição à palinologia dos cerrados. Academia Brasileira de Ciências, Rio de Janeiro.

Salgado, A.., Filho, S.J., Gonçalves, L., 1981. As Regiões fitoecológicas, sua natureza e seus recursos econômicos. Estudo fitogeográfico. Rio de Janeiro.

Schumm, S.A., 1977. The Fluvial System. John Wiley & Sons, New York.

Smith, C.B., Cohen, M.C.L., Pessenda, L.C.R., França, M.C., Guimarães, J.T.F., 2012. Holocenic proxies of sedimentary organic matter and the evolution of Lake Arari-Amazon Region. CATENA 90, 26–38.

Stuiver, M., Reimer, P.J., Reimer, R.W., 2017. CALIB 7.1.

Suguio, K., Barreto, A.M.F., Oliveira, P.E., Bezerra, F.H.R., Vilela, M.C.S.H., 2013. Indicators of Holocene sea level changes along the coast of the states of Pernambuco and Paraíba, Brazil. Geol. - Série Científica USP 13, 141–152.

Suguio, K., Martin, L., Bittencourt, A., 1985. Flutuações do nível relativo do mar durante o Quaternário Superior ao longo do litoral brasileiro e suas implicações na sedimentação costeira. Rev. Bras. Geociências 15, 273–286.

Thomas, R.G., Smith, D.G., Wood, J.M., Visser, J., Calverley-Range, E.A., Koster, E.H., 1987. Inclined heterolithic stratification—Terminology, description, interpretation and significance. Sediment. Geol. 53, 123–179.

Thornton, S.F., McManus, J., 1994. Application of Organic Carbon and Nitrogen Stable Isotope and C/N Ratios as Source Indicators of Organic Matter Provenance in Estuarine Systems: Evidence from the Tay Estuary, Scotland. Estuar. Coast. Shelf Sci. 38, 219–233.

Vedel, V., Behling, H., Cohen, M., Lara, R., 2006. Holocene mangrove dynamics and sea-level changes in northern Brazil, inferences from the Taperebal core in northeastern Pará State. Veg. Hist. Archaeobot. 15, 115–123.

Walker, R.G., 1992. Facies, facies models and modern stratigrahic concepts, in: Walker, R.G., James, N.P. (Eds.), Facies Models - Response to Sea Level Change. Geological Association of Canada, Ontario, p. 1–14.

Wentworth, C.K., 1922. A scale of grade and class terms for clastic sediments. J. Geol. 377–392.

Table 1. Sediment samples selected for radiocarbon dating with laboratory number, code site/
depth, 14C yr BP and calibrated (cal) ages.

Lab. Number (UGAMS)	Sample	Geographic position	Depth (cm)	Ages (^{14}C yr BP, 1σ)	Ages (cal yr BP, 2σ)	Mean (cal yr BP, 2σ)
21213	NAT1	S 5° 40' 36" W 35° 13' 37"	1,62 - 1,65	1820 +/- 20	1611 – 1745	1680
21214	NAT1		3,23 - 3,26	2140 +/- 20	2009 – 2114	2060
21215	NAT4	S 5° 40' 17" W 35° 14' 37"	1,07 - 1,10	1200 +/- 20	976 – 1094	1035
21216	NAT4		1,97 - 2,00	4070 +/- 25	4510 – 4628	4570
21217	NAT4		3,15 - 3,19	4130 +/- 25	4567 – 4728	4650
21218	NAT6	S 5° 40' 57" W 35° 14' 29",	1.71-1.75	6110 +/- 25	6831 – 7007	6920
21219	NAT8	S 5° 40' 16" W 35° 14' 2"	2.43-2.47	4520 +/- 25	5033 - 5290	5160

Table 2. Summary of facies association with sedimentary characteristics, predominance of pollen groups and geochemical data.

Facies association	Facies description	Pollen predominance	Geochemical data	Interpretation
A	Massive sand (facies Sm) with fine grain size and shell, cross-stratified sand (Scs), *Flaser* heterolithic bedding (Hf), olive gray color, and Inclined heterolithic stratification (IHS).	Trees, shrubs, mangrove and herbs	$\delta^{13}C$= -27.4 to -19‰ $\delta^{15}N$= 0.68 to 5.2‰ TOC= 0.9 to 15.5% TON= 0.03 to 0.4% C/N= 2 to 115	Tidal channel
B	Cross-stratified sand (Scs) with fine grain size, Wavy (Hw) lenticular heterolithic bedding (Hl) and small interval (10 cm) with massive mud (Mm).	Mangroves, trees and shrubs and herbs	$\delta^{13}C$= -27 to -24.3‰ $\delta^{15}N$= 0.26 to 6.2‰ TOC= 0.74 to 15.52% TON= 0.02 to 0.72% C/N= 14 to 68	Mangrove tidal flat
C	Wave lenticular bedding (Hw) with many bioturbation features such as woody roots, root marks and structures produced by the benthic fauna.	Trees and shrubs, herbs and mangrove	$\delta^{13}C$= -27.5 to -26,4‰ $\delta^{15}N$= 0.02 to 8.1‰ TOC= 3 to 14% TON= 0.01 to 0.13 C/N= 32 to 37	Herbs/mangrove mixed tidal flat
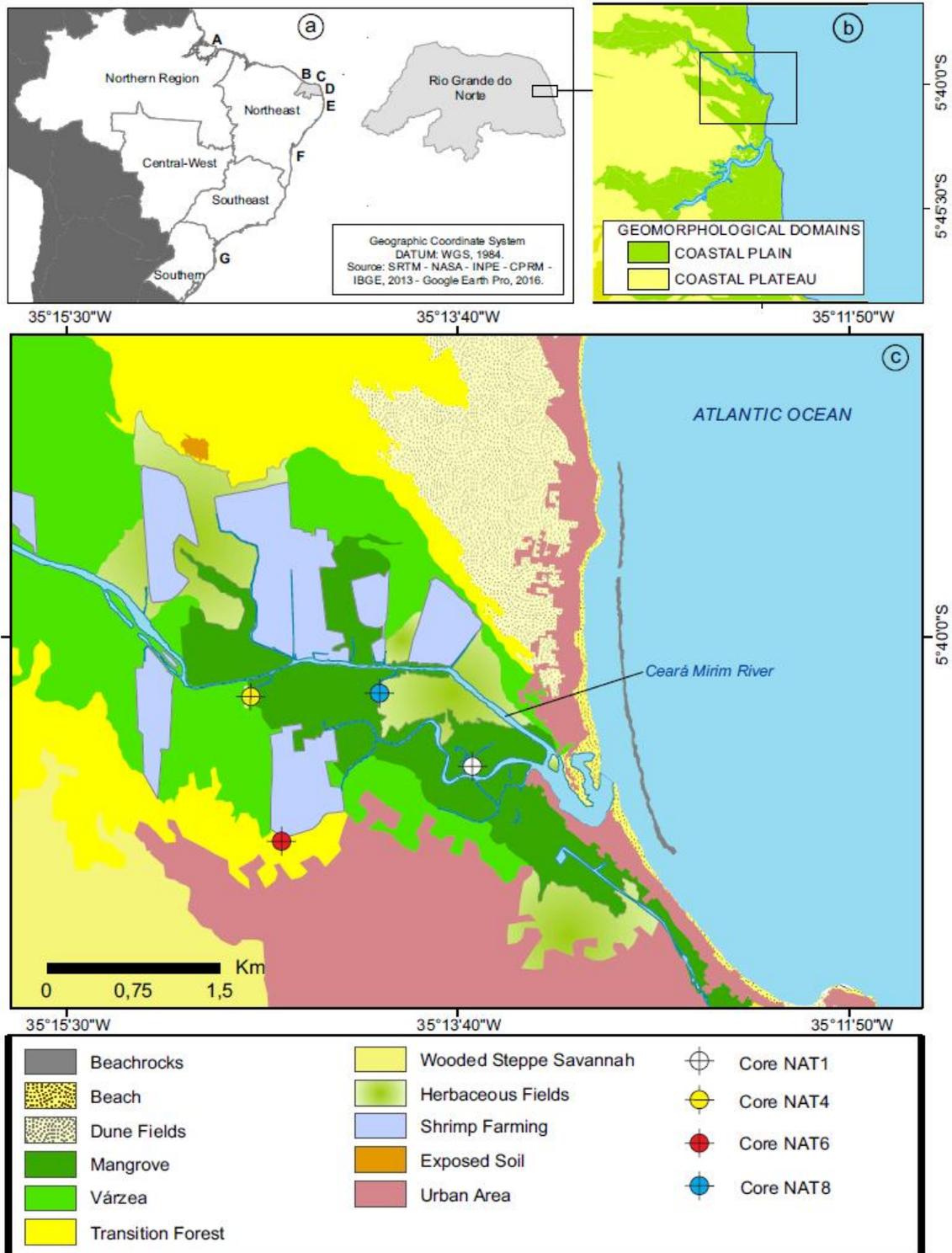
Figure 1. Scenes (1) Location of study area with Land Use/Land Cover and sampling sites of the cores; (2) Geomorphological features and (3) Brazilian regions and locations of the curves proposed for the sea-level.
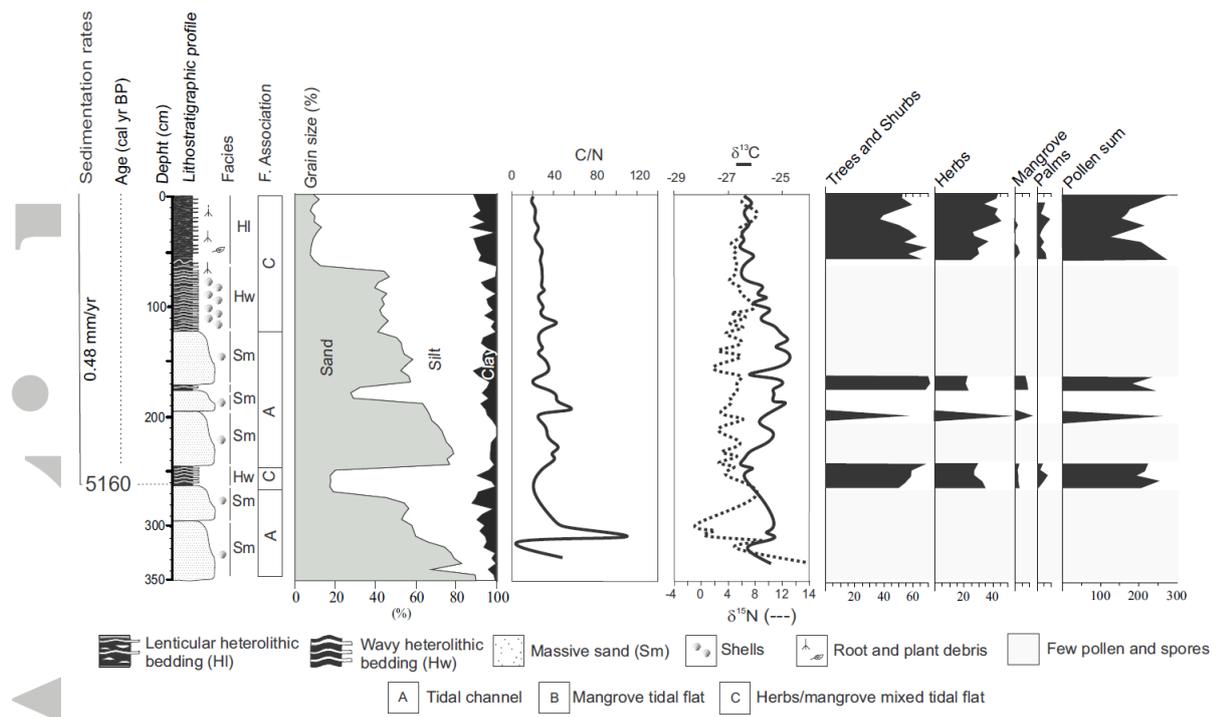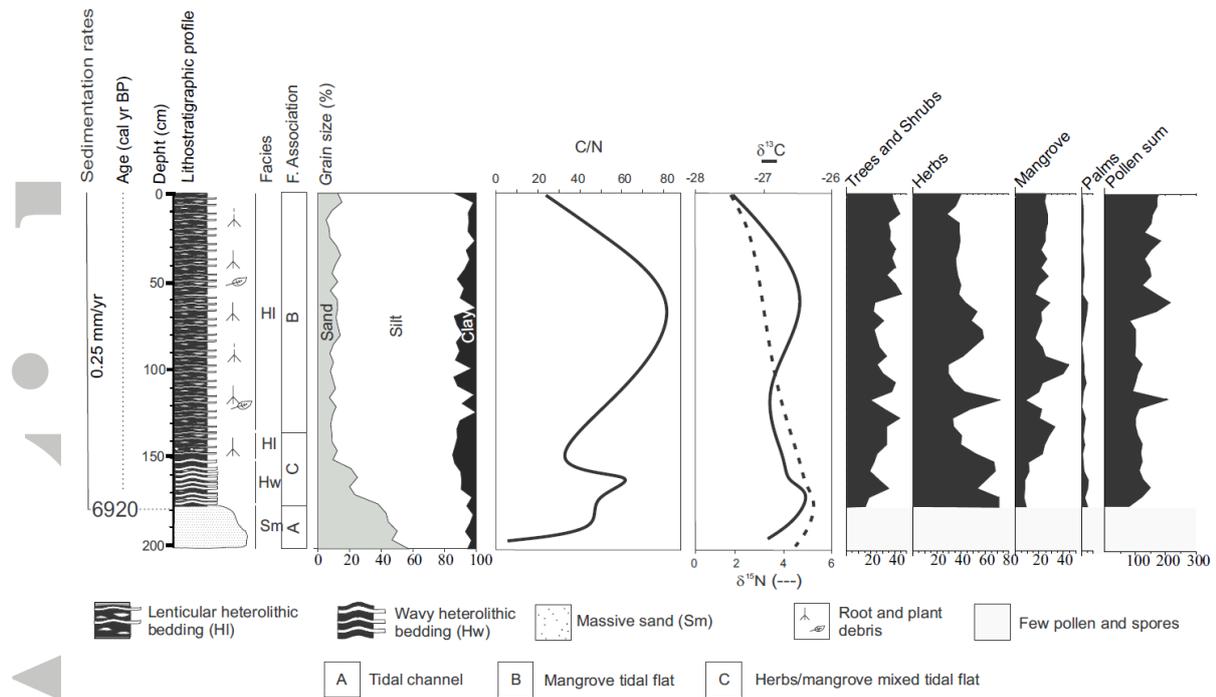
Figure 2. Summarized results for the core NAT8, with variation as a function of core depth showing chronological and lithological profiles with sedimentary facies, as well as ecological poll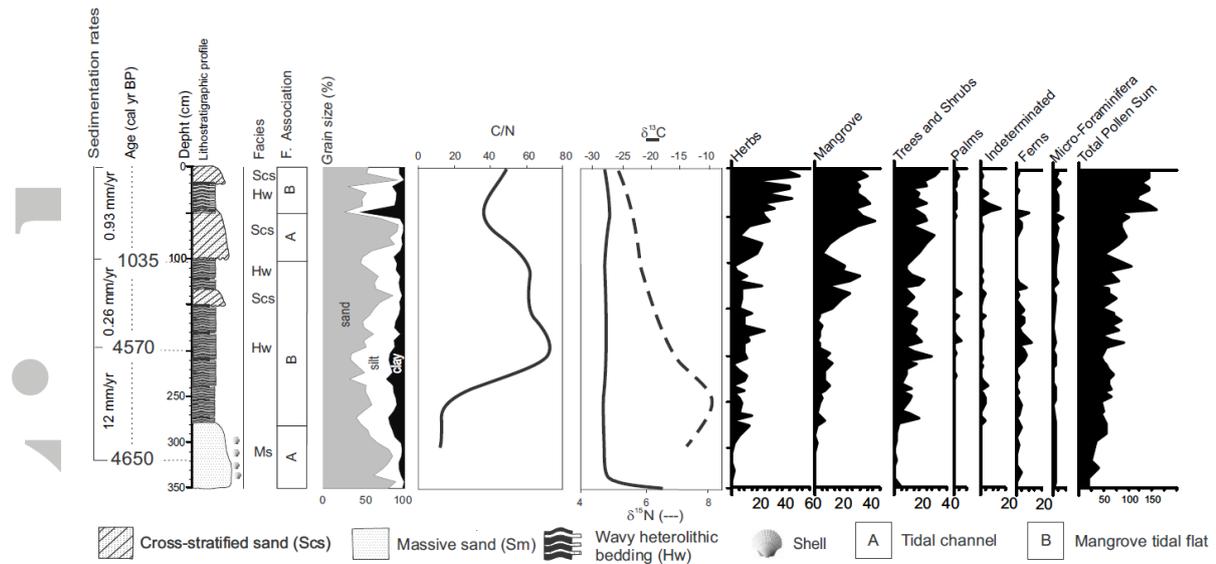en groups and geochemical variables. Pollen data are presented in the pollen diagrams as percentages of the total pollen sum.
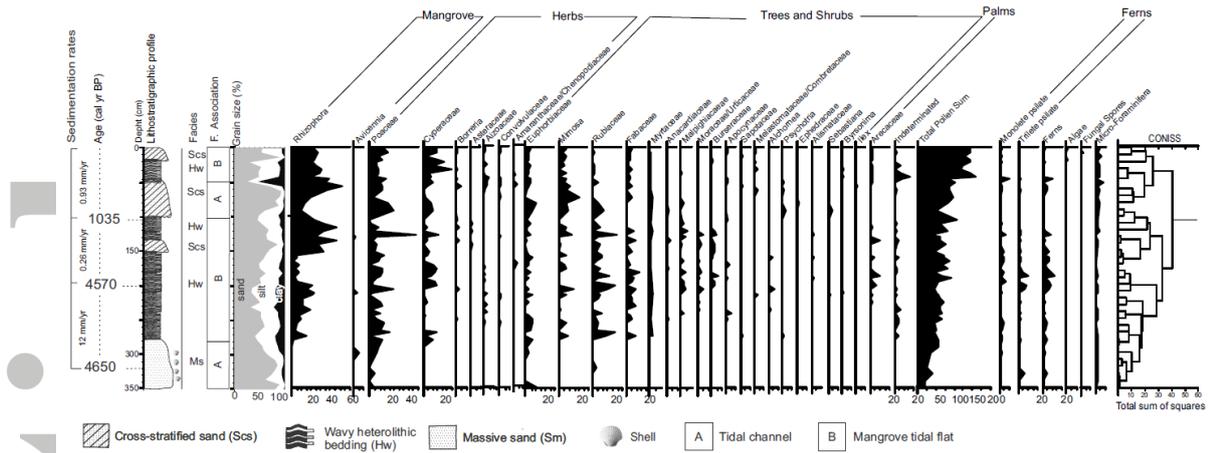
Figure 3. Pollen diagram of the core NAT8, with percentages of the most frequent pollen taxa, samples age and cluster analysis.

Figure 4. Summarized results for the core NAT6, with variation as a function of core depth showing chronological and lithological profiles with sedimentary facies, as well as ecological pollen groups and geochemical variables. Pollen data are presented in the pollen diagrams as percentages of the total pollen sum.
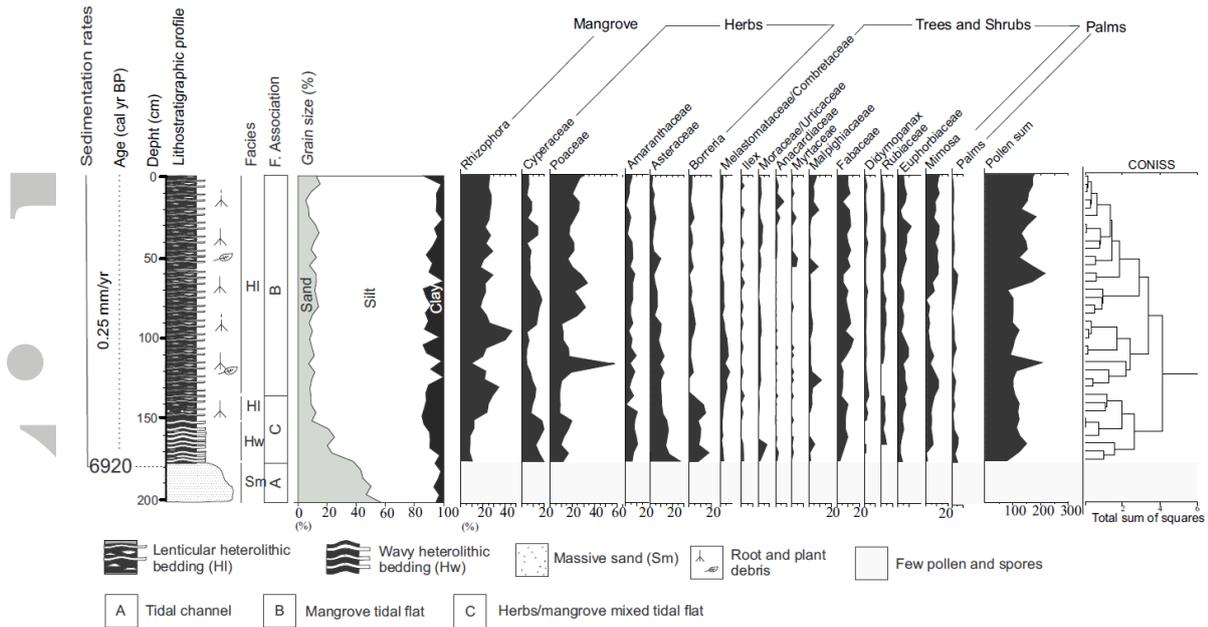
Figure 5. Pollen diagram of the core NAT6, with percentages of the most frequent pollen taxa, samples age and cluster analysis.
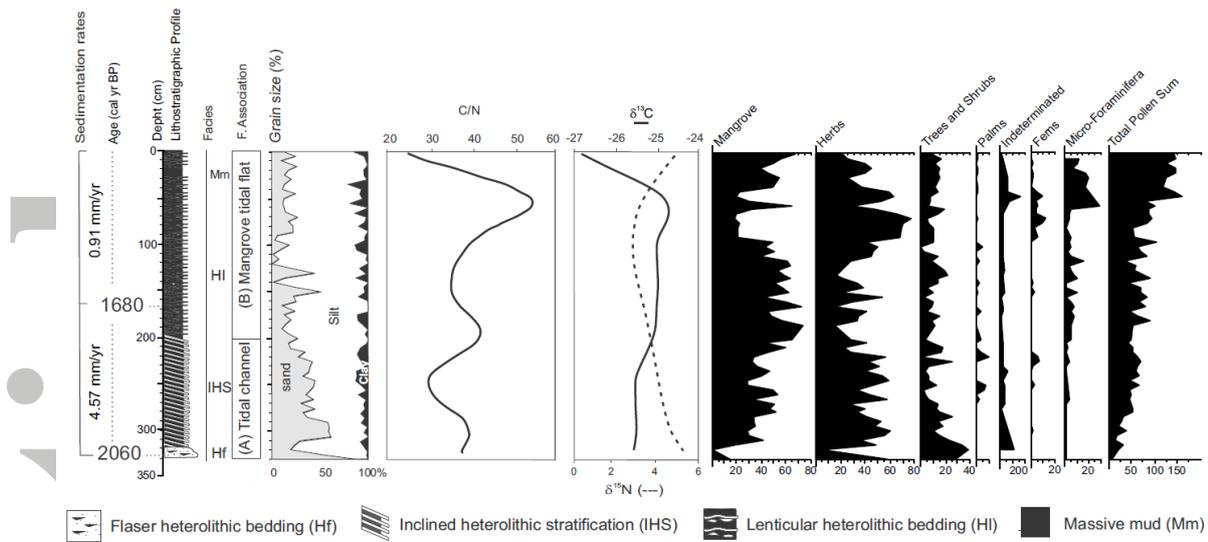
Figure 6. Summarized results for the core NAT4, with variation as a function of core depth showing chronological and lithological profiles with sedimentary facies, as well as ecological pollen groups and geochemical variables. Pollen data are presented in the pollen diagrams as percentages of the total pollen sum.

Figure 7. Pollen diagram of the core NAT4, with percentages of the most frequent pollen taxa, samples age and cluster analysis.

Figure 8. Summarized results for the core NAT1, with variation as a function of core depth showing chronological and lithological profiles with sedimentary facies, as well as ecological pollen groups and geochemical variables. Pollen data are presented in the pollen diagrams as percentages of the total pollen sum.

Figure 9. Pollen diagram of the core NAT1, with percentages of the most frequent pollen taxa, samples age and cluster analysis.
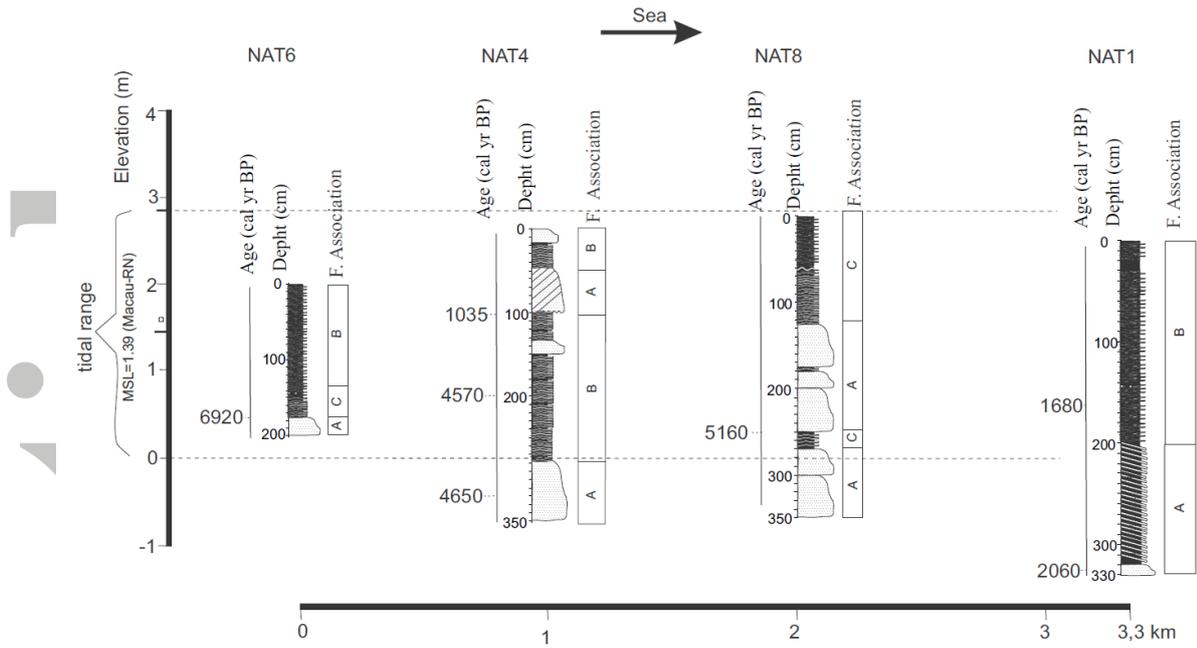
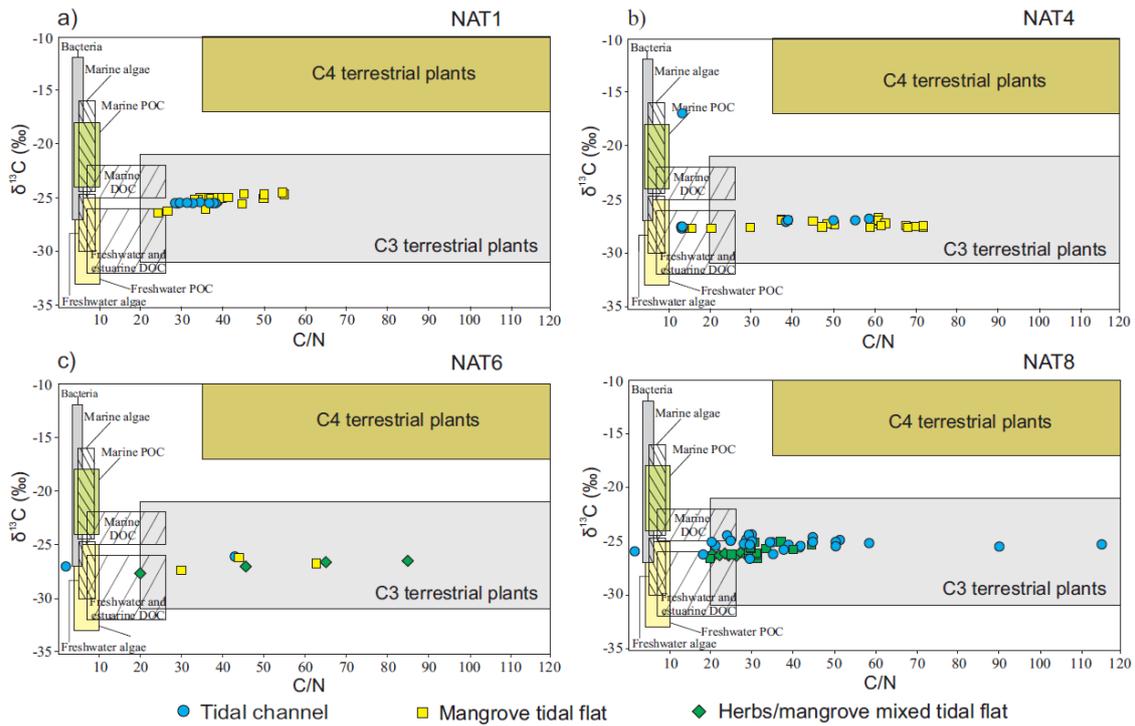Figure 10. Topographic correlation among the facies associations identified in the studied cores.

Figure 11. Binary diagram of $\delta^{13}C$ and C/N for the different facies associations (Tidal channel, Mangrove tidal flat and Herbaceous/mangrove mixed tidal flat) with interpretation according to data presented by Lamb et al. (2006), Meyers (2003) and Wilson et al. (2005).
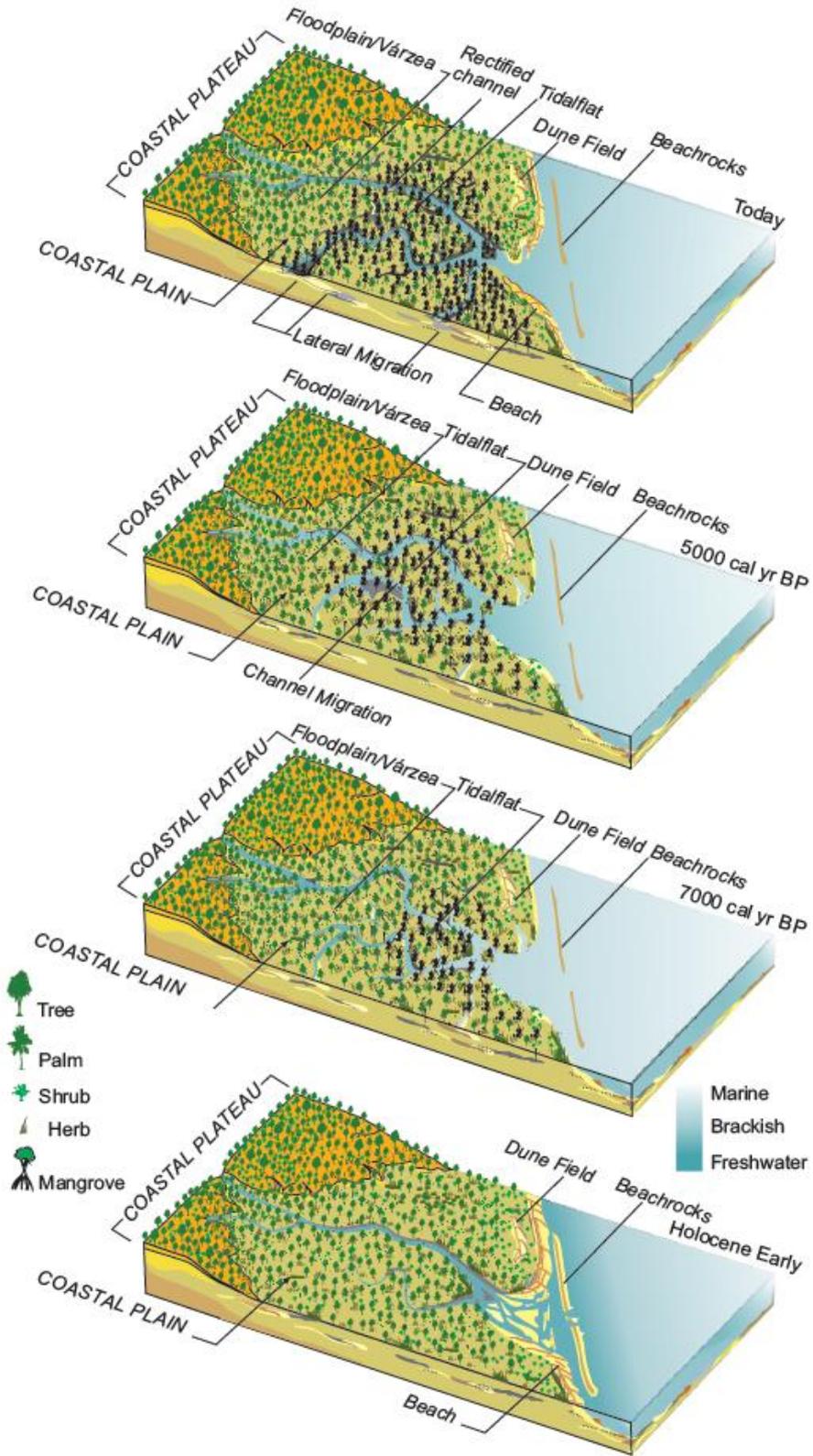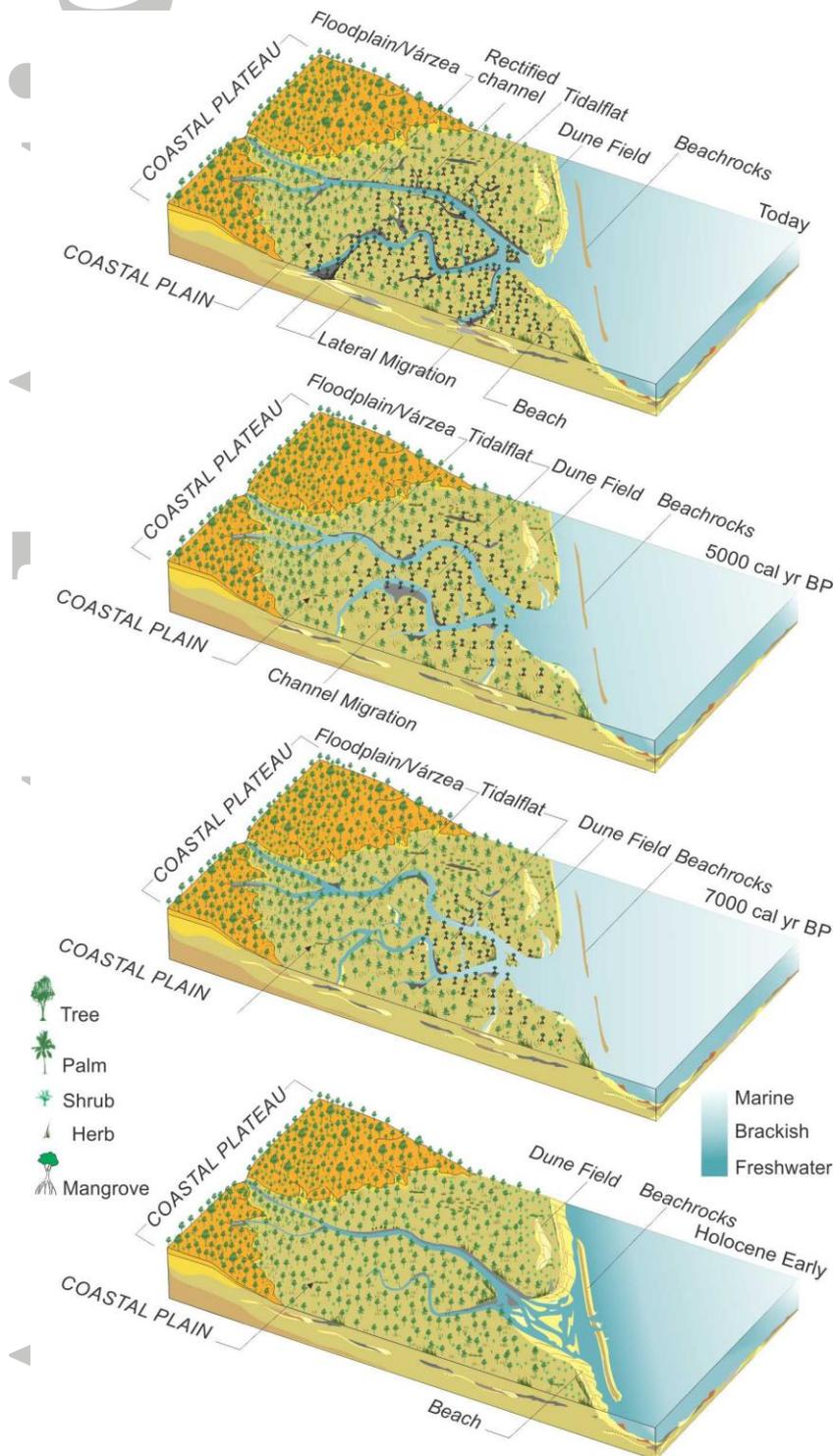
Figure 12. Schematic representation of successive phases the mangrove establishment according to sea-level change and active channel and lateral migration.

Allogenic and autogenic effects on mangrove dynamics from the Ceará Mirim River, Northeastern Brazil, during the middle and late Holocene

Samuel R. Ribeiro, Edson J.L Batista, Marcelo C.L. Cohen[*], Marlon C. França, Luiz C.R. Pessenda, Neuza A. Fontes, Igor C. C. Alves[a], José A. Bendassolli

Schematic representation of successive phases of mangrove establishment according to sea-level change and lateral migration of channels.